International Journal of Mass Spectrometry and Ion Processes, 113 (1992) 1–12
Elsevier Science Publishers B.V., Amsterdam

Cross-sections for electron impact ionization of O_2

E. Krishnakumar[1] and S.K. Srivastava
Jet Propulsion Laboratory, California Institute of Technology, 4800 Oak Grove Drive, Pasadena CA 91109 (USA)

(First received 6 March 1991; in final form 28 June 1991)

ABSTRACT

Using a crossed electron beam–molecular beam collision geometry and the relative flow technique measurements have been made to generate a uniform set of electron impact ionization cross-section data for O_2 for electron impact energies from threshold to 1000 eV. Present values of total, partial and dissociative ionization cross-sections are compared with previously published data. Cross-sections for the formation of O^{2+} from O_2 have been measured for the first time.

Keywords: cross-sections; O_2; O^{2+}; electron impact ionization.

INTRODUCTION

The dissociative ionization of molecules resulting in the formation of atomic ions or other positively charged fragments is a very important aspect of the dynamics of the ionization of the molecules. Even though measurements on the cross-sections for ionization of molecules have been carried out for more than 50 years, very little effort has been directed at measuring them for the dissociative ionization process [1]. Moreover, whatever measurements have been performed have been less than satisfactory. The main reason for this situation has been the technical difficulty caused by the initial kinetic energies of ions resulting from the dissociative ionization process. These initial kinetic energies hinder the complete collection of fragment ions from the ionization region. However, recent developments of a fast beam technique [2] and a pulsed ion extraction technique [3] have provided satisfactory results. In this paper we report ionization cross-sections for O_2 which have been obtained by utilizing this latter technique.

The dissociative ionization process resulting from electron impact on O_2 has been studied by several authors in the past. Hagstrum [4], Ehrhardt and Kresling [5], Stockdale and Deleanu [6], and Locht and Schopman [7] all

[1] Permanent address: Tata Institute of Fundamental Research, Homi Bhabha Road, Bombay 400 005, India.

0168-1176/92/$05.00

investigated kinetic energy spectra of O^+ ions and correlated these with the various possible channels in the dissociative ionization process. Freund [8] has reported the kinetic energy distribution of metastable and highly excited Rydberg oxygen atoms. Brehm and DeFrenes [9] studied the formation of O^{2+} via the channel

$$O_2 + e^- \longrightarrow O^+ + O^+ + 3e^- \quad (1)$$

Measurements of absolute values of cross-sections for the ionization of O_2 by electron impact have mostly been confined to the total ionization cross-sections (i.e. weighted sum of all direct and partial ionization cross-sections). These measurements have been carried out by Tate and Smith [10], Craggs et al. [11], Schulz [12], Asundi et al. [13], Rapp and Englander-Golden [14], and Peresse and Tuffin [15] for various electron impact energy ranges from threshold to 1000 eV. Schram et al. [16] have measured values of total cross-sections for electron impact energies up to 20 keV. Partial cross-sections have been reported by Peresse and Tuffin [15] and by Märk [17]. Cross-sections for the dissociative ionization process have been measured by Peresse and Tuffin [15] and by Rapp et al. [18]. Recently Evans et al. [19] have reported cross-sections for the formation of O_2^+ and O^+ from the ground state as well as from the vibrationally excited state. Cross-sections for the formation of O^{2+} have not been reported so far.

A careful examination of previous data on partial and dissociative ionization cross-sections shows that there are large disagreements between the various results. This prompted us to undertake a systematic study of the electron impact ionization properties of O_2.

EXPERIMENTAL APPARATUS AND METHOD OF DATA REDUCTION

A schematic diagram of the apparatus used in the present measurements is shown in Fig. 1. This apparatus, the method of data acquisition and the procedure for obtaining normalised values of cross-sections have been described previously (ref. 3 and references cited therein). In the present measurements, however, we have added, to the existing apparatus, a time-of-flight mass spectrometer (TOFMS) in addition to the quadrupole mass spectrometer (QMS) as shown in Fig. 1. This modification was motivated by the fact that, for our applications, a TOFMS has some advantages over the QMS. First, the TOFMS eliminates, to a great extent, uncertainties in the relative values of ion intensities caused by high kinetic energies of ions formed in the dissociative ionization process. This was verified by calculating trajectories of ions through the TOFMS for ions with kinetic energies up to 5 eV. Results of these trajectory calculations have been reported previously in ref. 3. Second, if properly designed and operated, the transmission efficiency of the TOFMS

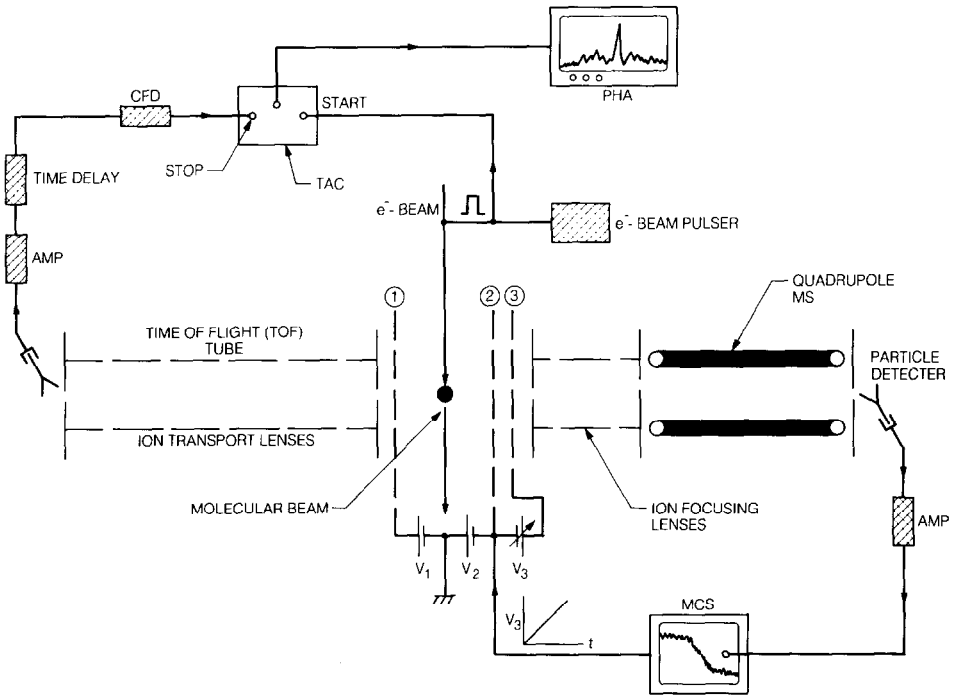

Fig. 1. Schematic of the experimental arrangement.

can be made completely independent of mass/charge ratios of ions. In practice this condition is very difficult to obtain for the QMS. Third, the TOFMS can record all ion intensities simultaneously. Therefore, rapid changes in the conditions of the ion source do not affect the relative intensities of ions with different mass/charge ratios. Fourth, the TOFMS has a better resolution for low mass/charge ratios than the QMS which is the subject of a current investigation.

Our TOFMS consists of five electrostatic cylindrical lenses of 25 mm diameter and of varying lengths. The overall flight length is 200 mm. Ions are extracted from the ionization region by a pulse of about 50 V cm^{-1}. They are transported through the electrostatic lenses and are subsequently focused at a channel electron multiplier. Each incident ion gives rise to an electrical pulse which is amplified by a fast amplifier.

The time-of-flight spectrum is generated in the following way . A synchronous pulse from the pulse generator, used for the electron beam pulsing, is fed into the start terminal of a time-to-amplitude converter (TAC). This starts a clock in the TAC. The output pulse from the amplifier is fed to a constant fraction discriminator (CFD). The output of the CFD is then applied, after a suitable time delay, to the stop input of the TAC. The time difference

between the two pulses (input and output) is converted into an electrical pulse whose amplitude is directly proportional to the time difference. The output pulses of varying amplitudes are stored in a pulse height analyser (PHA). The time-of-flight spectrum thus generated can be converted into a mass/charge spectrum with the aid of a simple computer program.

In our experiment a specific mass peak from the TOFMS spectrum was selected by using a combination of proper delay times of start and stop pulses. The output of the TAC was then applied to a multichannel scaler (MCS). A voltage ramp from the MCS was used to change the electron impact energy in regular intervals of 0.5 eV. A record of the intensity of a specific ion vs. the electron impact energy is called the ionization efficiency curve. This curve was obtained for each ionic species of present interest. The ionization efficiency curves obtained in this way were then normalised to yield absolute values of cross-sections by using the relative flow technique (details are given in ref. 3 and the references cited therein). However, we will briefly describe this technique here for the sake of clarity. First, the energy of the electron beam is fixed at some value. In the present case it was fixed at 100 eV. At the same time a beam of He atoms is generated by flowing He gas through a capillary array [20]. The gas pressure behind the capillary array is kept at a value which produces a semi-molecular flow of the gas through the capillary array. Theoretical equations describing this flow have been derived by Brinkman and Trajmar [21] and their validity has been tested by several previous experimental measurements. The number of counts per second of He^+ ions is then recorded. After this, the beam of He atoms is turned off and is replaced by O_2 molecules by flowing O_2 gas through the capillary array. Again, the pressure behind the capillary array is adjusted to a value which is within the limits set by the condition of semi-molecular flow. Number of counts per second of O_2^+, $O^+ + O_2^{2+}$, and O^{2+} are then recorded. During these measurements all other experimental conditions, such as electron beam current, ion extraction voltages, etc., are kept constant. The two counting rates can be related to each other by the following equation:

$$\sigma_u(E_0) = \sigma_{He}(N_u/N_{He})(M_{He}/M_u)^{1/2}(F_{He}/F_u)(K_{He}/K_u) \tag{2}$$

where σ_u is the cross-section of the unknown gas, σ_{He} is the cross-section for the ionization of He atoms, N_u and N_{He} are the ion counting rates for the unknown and for He gas respectively, M_{He} and M_u are the atomic and molecular weights of the two gases, F_{He} and F_u are the flow rates of the two gases through the capillary array, and K_{He} and K_u are the transmission and detection efficiencies for two gaseous ions through the entire apparatus and through the channeltron respectively.

Details of the method for measuring the flow rates are given in ref. 20. The procedure for obtaining the values of K_{He} and K_u has been described in ref. 22

and will be briefly presented here. For this purpose eqn. 2 is employed. The rare gases He, Ne, Ar, Kr, and Xe are flowed through the capillary array and their ion intensities (e.g. N_{He}) are recorded at a fixed electron impact energy. These intensities are substituted into eqn. 2. Cross-sections for single ionization of rare gases [23,24] are accurately known. Thus, from eqn. 2 K_{He}/K_u ratios, where u represents other rare gases, are obtained. Ratios K_{He}/K_u are then plotted as a function of mass. Between the data points an interpolation is made and K_{He}/K_u ratios of present interest (i.e. for the various ions of O_2) are obtained. By utilizing the SIMION program for calculating the ion trajectories through the time-of-flight system we have determined that the transmission efficiency is independent of the charge state of the ions.

Experimental measurements over a period of several months and under different experimental conditions produced ionization efficiency curves which agreed in shape with each other within 5%. The values of σ_{He} used in the present work for normalizing the data were recommended by Bell et al. [23] and are known with an accuracy of 5%. The ratios of counting rates N_u/N_{He} are obtained with an accuracy of about 2%. The flow rates F_{He}/F_u are measured with an accuracy of 5%. The ratios of counting rates N_u/N_{He} are obtained with an accuracy of about 2%. The flow rates F_{He}/F_u are measured with an accuracy better than 5% and the ratios K_{He}/K_u are estimated to be of the order of 10% accuracy. Therefore, a square root of the sum of squares of individual errors results in a value of about 13% for the error in the cross-section data reported in this paper.

RESULTS AND DISCUSSION

Present results are given in Table 1. Previous data and our measurements are shown in Figs. 2–4 and are discussed below.

Direct ionization cross-sections

In Fig. 2 we present cross-section data of Peresse and Tuffin [15], Märk [17], and Evans et al. [19] along with our own. Results of Peresse and Tuffin are substantially higher than the present ones and others. Measurements of Märk and Evans et al., however, are lower by more than the error limits of the present data. Above the electron impact energy of 350 eV there are no experimental results except ours.

Dissociative ionization cross-sections

Figure 3 shows present results along with previously measured cross-sections for the dissociative ionization (i.e. $e^- + O_2 \rightarrow O^+ + O + 2e^-$) and

TABLE 1

Partial and total ionisation cross-sections for O_2 by electron impact

Electron energy (eV)	O_2^+ (10^{-18} cm^2)	$O^+ + O_2^{2+}$ (10^{-18} cm^2)	O^{2+} (10^{-18} cm^2)	Total (10^{-18} cm^2)
13.0	2.0	0.0	0.0	2.0
14.0	4.1	0.0	0.0	4.1
15.0	6.5	0.0	0.0	6.5
16.0	10.9	0.0	0.0	10.9
17.0	15.8	0.0	0.0	15.8
18.0	20.3	0.19	0.0	20.5
19.0	24.6	0.27	0.0	24.9
20.0	28.8	0.48	0.0	29.3
22.5	42.0	1.80	0.0	43.8
25.0	51.9	4.20	0.0	56.1
27.5	61.8	7.80	0.0	69.6
30.0	69.3	11.5	0.0	80.8
32.5	77.2	16.2	0.0	93.4
35.0	86.1	22.8	0.0	108.9
40.0	104.1	32.2	0.0	136.3
45.0	120.6	40.8	0.0	161.4
50.0	134.4	48.0	0.0	182.4
53.0	–	–	0.0	–
54.0	–	–	0.0	–
55.0	148.0	55.8	0.0005	203.8
56.0	–	–	0.0012	–
57.0	–	–	0.0017	–
58.0	–	–	0.0020	–
59.0	–	–	0.0024	–
60.0	153.8	63.1	0.0029	216.9
61.0	–	–	0.0033	–
62.0	–	–	0.0036	–
63.0	–	–	0.0041	–
64.0	–	–	0.0053	–
65.0	161.8	70.7	0.0080	–
66.0	–	–	0.0111	–
67.0	–	–	0.0162	–
68.0	–	–	0.021	–
69.0	–	–	0.029	–
70.0	169.2	76.2	0.039	245.5
75.0	174.6	81.8	0.107	256.6
80.0	179.5	86.6	0.21	266.5
85.0	184.1	89.0	0.30	273.7
90.0	187.9	91.9	0.41	281.0

TABLE 1 (continued)

Electron energy (eV)	O_2^+ (10^{-18} cm^2)	$O^+ + O_2^{2+}$ (10^{-18} cm^2)	O^{2+} (10^{-18} cm^2)	Total (10^{-18} cm^2)
95.0	190.5	94.7	0.52	286.2
100.0	192.3	97.2	0.63	290.8
105.0	193.3	99.1	0.74	293.9
110.0	193.4	100.7	0.86	295.9
115.0	193.3	102.0	0.98	297.3
120.0	192.8	102.8	1.11	297.8
125.0	192.0	103.4	1.24	297.5
130.0	190.8	103.7	1.35	297.2
135.0	189.6	104.0	1.52	296.6
140.0	188.2	104.3	1.66	295.8
145.0	186.6	104.4	1.80	294.6
150.0	185.3	104.2	1.91	294.3
155.0	184.1	103.9	2.02	292.0
160.0	182.3	103.6	2.12	290.1
165.0	180.8	103.2	2.21	288.4
170.0	179.3	102.8	2.29	286.7
175.0	178.0	102.1	2.36	284.8
180.0	176.7	101.8	2.43	283.4
185.0	175.3	101.0	2.50	281.3
190.0	174.0	100.4	2.55	279.4
195.0	172.1	99.7	2.60	277.0
200.0	170.3	99.0	2.64	274.6
210.0	167.4	97.6	2.73	270.5
220.0	165.0	96.0	2.80	266.6
230.0	162.8	94.2	2.83	262.6
240.0	159.8	92.5	2.84	258.0
250.0	156.9	90.7	2.84	253.3
260.0	154.7	89.0	2.83	249.4
270.0	152.0	87.3	2.81	244.9
280.0	149.4	85.6	2.77	240.5
290.0	147.3	84.0	2.72	236.7
300.0	145.6	82.0	2.68	233.0
350.0	135.5	74.2	2.46	214.6
400.0	126.2	67.2	2.22	197.8
450.0	118.8	60.9	2.00	183.7
500.0	111.2	56.2	1.81	171.0
550.0	105.8	52.1	1.65	161.2
600.0	99.9	48.7	1.53	151.7
650.0	94.5	45.6	1.41	142.9
700.0	90.0	43.0	1.32	135.6

TABLE 1 (continued)

Electron energy (eV)	O_2^+ (10^{-18} cm^2)	$O^+ + O_2^{2+}$ (10^{-18} cm^2)	O^{2+} (10^{-18} cm^2)	Total (10^{-18} cm^2)
750.0	85.8	40.7	1.23	129.0
800.0	81.9	38.5	1.15	122.7
850.0	78.3	36.5	1.09	117.0
900.0	75.5	34.9	1.01	112.4
950.0	72.8	33.6	0.95	108.3
1000.0	70.5	33.0	0.94	105.4

double ionization (i.e. $e^- + O_2 \rightarrow O_2^{2+} + 3e^-$) processes. Since the mass spectrometer measures $m/z = 16$, which is the same for both O^+ and O_2^{2+}, the cross-sections for the production of O^+ are actually the sum of O^+ and O_2^{2+}. The only way to distinguish the O^+ ion from the O_2^{2+} ion is to use isotopically-enriched O_2. Märk [17] has measured cross-sections for the production of O_2^{2+} and finds that they are less than 1% of those for the production of O_2^+. Cross-sections measured by Rapp et al. [18] are in excellent agreement with the present results. Data reported by Peresse and Tuffin [15] agree well with

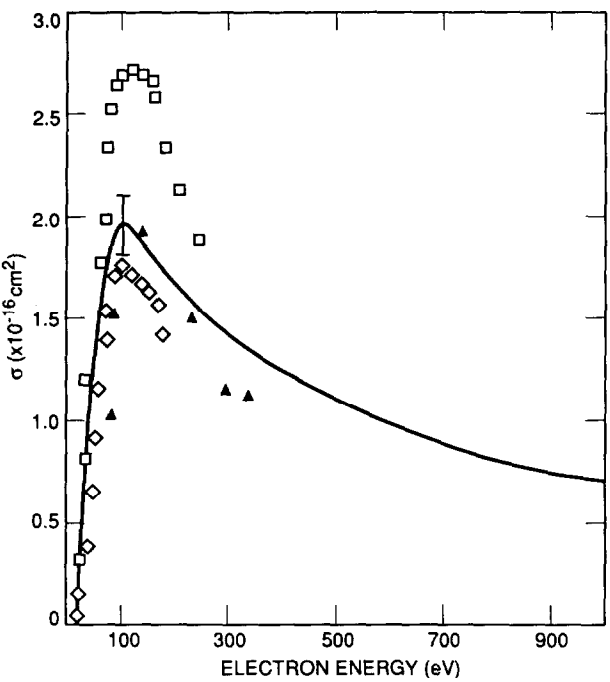

Fig. 2. Cross-sections for the process $e^- + O_2 \rightarrow O_2^+ + 2e^-$: (□), Peresse and Tuffin [15]; (◇), Märk [17]; (▲), Evans et al. [19], (——), present data.

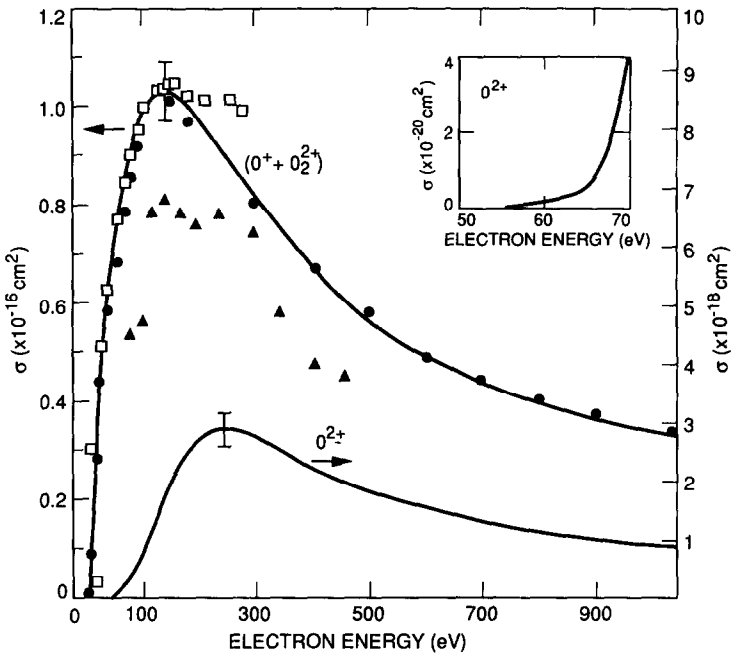

Fig. 3. Dissociative ionization cross-sections: (●), Rapp et al. [18]; (□), Peresse and Tuffin [15] (their data have been multiplied by a factor of seven); (▲), Evans et al. [19]; (——), present data. The Y axis scale for O^{2+} data is given on the right-hand side.

ours in shape but are very different in magnitude. In Fig. 3 we have shown their data after multiplying them by a factor of seven. Evans et al. [19] have reported cross-sections for this process which are considerably lower than the present results. In addition, their data show structure in the ionization efficiency curve which is seen neither in the present measurements nor in the data reported by Rapp et al.

In Fig. 3 cross-sections for the production of O^{2+} are also shown. There are no previous data to compare with the present results. The inset shows the threshold region in detail. From this it can be seen that the ionization efficiency curve has a threshold of approximately 54 eV followed by a sudden rise at about 63 eV indicating a second threshold. This leads to the conclusion that there are two distinct processes giving rise to the formation of the O^{2+} ion. A comparison of the slopes of the two curves shows that the first process is weaker compared to the second one. We propose the formation of O^{2+} through the following channels:

$$e^- + O_2 \longrightarrow O_2^{2+} + 3e^- \longrightarrow O + O^{2+} + 3e^- \qquad (2)$$

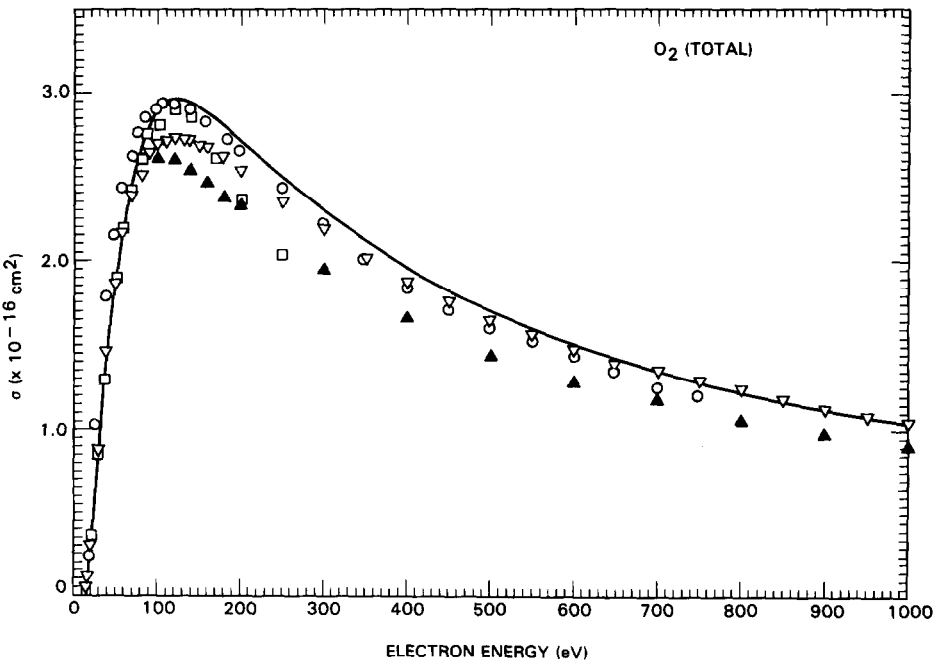

Fig. 4. Total ionization cross-sections; (▽), Rapp and Englander-Golden [14]; (▲), Schram et al. [16]; (○), Tate and Smith [10]; (□), Peresse and Tuffin [15]; (——), present data. Not shown are the results of Craggs et al. [11], Schulz [12], and Asundi et al. [13] (see text).

and

$$e^- + O_2 \longrightarrow O_2^{3+} + 4e^- \longrightarrow O^+ + O^{2+} + 4e^- \qquad (3)$$

The threshold for the first process has been reported by Daley and Powell [24] as 52.7 ± 0.5 eV. Since in our measurements we have an uncertainty of about 1 eV, this value agrees well with ours. The threshold of the second process is estimated to be 63 ± 2 eV. It is surprising to note that the cross-sections for the formation of O^{2+} are being dominated by the second process considering the fact that the probability of formation of triply charged molecular ion should be much less than that of the doubly charged ion. O_2^{2+} is bound by a localised potential well situated above the dissociation limit for the production of two O^+ ions simultaneously. It is metastable in nature and eventually dissociates into two O^+ ions via the process of quantum mechanical tunneling across the potential barrier. The lifetime for this will depend on its vibrational and rotational excitations and the nature of the potential barrier itself. This can easily be of the order of tens of microseconds which is typically the flight time of the ions from the ionization region to the detector.

Therefore, most of the O^{2+} generated by the process represented by eqn. 2 may escape detection by our experimental arrangement.

Total cross-sections

Present results are shown in Fig. 4 along with previous measurements by Tate and Smith [10], Rapp and Englander-Golden [14], Schram et al. [16], and Peresse and Tuffin [15]. Cross-section data published by Craggs et al. [11], Schulz [12], and Asundi et al. [13] are not given here because they agree very well with the results of Tate and Smith. As can be seen in the figure our data are higher than the cross-section values of Rapp and Englander-Golden in the electron impact energy range between about 70 eV and 500 eV. However, within the error limits of the two experiments the agreement is satisfactory. It is interesting to note that present results are in excellent agreement with the older results of Tate and Smith over the entire electron impact energy range. The data reported by Schram et al. are much lower in magnitude than ours and lie outside the error limits. Measurements of Peresse and Tuffin agree with the present results over a very limited electron impact energy range and at higher energies they appear to be falling very rapidly.

ACKNOWLEDGMENTS

The research described in this paper was carried out at the Jet Propulsion Laboratory, California Institute of Technology, under contract with the U.S. Airforce Office of Scientific Research and the National Aeronautic and Space Administration. E.K. thanks the National Research Council, Washington, DC for a Resident Research Associateship grant during the course of this work.

REFERENCES

1 T.D. Märk, in T.D. Märk and G.H. Dunn (Eds.), Electron Impact Ionization, Springer-Verlag, Vienna, 1985, pp. 137–197.
2 F.A. Baiocchi, R.C. Wetzel and R.S. Freund, Phys. Rev. Lett., 53 (1984) 771.
3 E. Krishnakumar and S.K. Srivastava, J. Phys. B, 23 (1990) 1893.
4 H.D. Hagstrum, Rev. Mod. Phys., 23 (1951) 185.
5 H. Ehrhardt and A. Kresling, Z. Naturforsch., Teil A, 22 (1967) 2036.
6 J.A.D. Stockdale and L. Deleanu, Chem. Phys. Lett., 22 (1973) 204.
7 R. Locht and J. Schopman, Int. J. Mass Spectrom. Ion Phys., 15 (1974) 361.
8 R.S. Freund, J. Chem. Phys., 54 (1971) 3125.
9 B. Brehm and G. DeFrenes, Int. J. Mass Spectrom. Ion Phys., 26 (1978) 251.
10 J.T. Tate and P.T. Smith, Phys. Rev., 39 (1932) 270.
11 J.D. Craggs, R. Thorburn and B.A. Tozer, Proc. R. Soc. London, Ser. A, 240 (1957) 473.
12 G.J. Schulz, Phys. Rev., 128 (1962) 178.

13 R.K. Asundi, J.D. Craggs and M.V. Kurepa, Proc. Phys. Soc. (London), 82 (1963) 967.
14 D. Rapp and P. Englander-Golden, J. Chem. Phys., 43 (1965) 1464.
15 J. Peresse and F. Tuffin, Methodes Phys. Anal., 3 (1967).
16 B.L. Schram, F.J. deHeer, M.J. van der Wiel and J. Kistemaker, Physica, 31 (1964) 94.
17 T.D. Märk, J. Chem. Phys., 63 (1975) 3731.
18 D. Rapp, P. Englander-Golden and D.D. Briglia, J. Chem. Phys., 42 (1965) 4081.
19 B. Evans, J.S. Chang, A.W. Yan, R.W. Nicholls and R.M. Hobson, Phys. Rev. A, 38 (1988) 2782.
20 S.K. Srivastava, A. Chutjian and S. Trajmar, J. Chem. Phys., 63 (1975) 2659.
21 R.T. Brinkman and S. Trajmar, J. Phys. E, 14 (1981) 245.
22 E. Krishnakumar and S.K. Srivastava, J. Phys. B, 21 (1988) 1055.
23 K.L. Bell, H.B. Gilbody, J.G. Hughs, A.E. Kingston and F.J. Smith, J. Phys. Chem. Ref Data, 12 (1983) 891.
24 N.R. Daley and R.E. Powell, Proc. Phys. Soc. (London), 90 (1967) 629.